ISSN 1674-1056
http://cpb.iphy.ac.cn
http://iopscience.iop.org/cpb
中国物理 B
Chinese Physics
中国物理 Chinese Physics B

Extraordinary transmission and reflection in *PT*-symmetric two-segment-connected triangular optical waveguide networks with perfect and broken integer waveguide length ratios

Jia-Ye Wu(吴嘉野), Xu-Hang Wu(吴栩航), Xiang-Bo Yang(杨湘波), Hai-Ying Li(李海盈)
Citation: Chin. Phys. B . 2019, 28(10): 104208 . **doi:** 10.1088/1674-1056/ab3f92
Journal homepage: http://cpb.iphy.ac.cn; http://iopscience.iop.org/cpb

What follows is a list of articles you may be interested in

Dynamics of Airy beams in parity-time symmetric optical lattices

Rui-Hong Chen(陈睿弘), Wei-Yi Hong(洪伟毅)
Chin. Phys. B . 2019, 28(5): 054202 . **doi:** 10.1088/1674-1056/28/5/054202

Fundamental and dressed annular solitons in saturable nonlinearity with parity-time symmetric Bessel potential

Hong-Cheng Wang(王红成), Ya-Dong Wei(魏亚东), Xiao-Yuan Huang(黄晓园), Gui-Hua Chen(陈桂华), Hai Ye(叶海)
Chin. Phys. B . 2018, 27(4): 044203 . **doi:** 10.1088/1674-1056/27/4/044203

Bifurcated overtones of one-way localized Fabry–Pérot resonances in parity-time symmetric optical lattices

Fatma Nafaa Gaafer, Yaxi Shen(沈亚西), Yugui Peng(彭玉桂), Aimin Wu(武爱民), Peng Zhang(张鹏), Xuefeng Zhu(祝雪丰)
Chin. Phys. B . 2017, 26(7): 074218 . **doi:** 10.1088/1674-1056/26/7/074218

The contrast between defect solitons in parity–time symmetric superlattice and simple-lattice complex potentials

Hu Su-Mei,Hu Wei
Chin. Phys. B . 2012, 21(2): 024212 . **doi:** 10.1088/1674-1056/21/2/024212

Extraordinary transmission and reflection in $\mathcal{PT}$-symmetric two-segment-connected triangular optical waveguide networks with perfect and broken integer waveguide length ratios*

Jia-Ye Wu(吴嘉野)[1,2,†], Xu-Hang Wu(吴栩航)[1,†], Xiang-Bo Yang(杨湘波)[1,‡], and Hai-Ying Li(李海盈)[1]

[1] *Guangzhou Key Laboratory for Special Fiber Photonic Devices, School of Information and Optoelectronic Science and Engineering, South China Normal University, Guangzhou* 510006, *China*

[2] *Laboratory of Nonlinear Fiber Optics, School of Electronic and Computer Engineering, Peking University, Shenzhen* 518055, *China*

(Received 10 June 2019; revised manuscript received 17 July 2019; published online 25 September 2019)

By adjusting the waveguide length ratio, we study the extraordinary characteristics of electromagnetic waves propagating in one-dimensional (1D) parity-time-symmetric ($\mathcal{PT}$-symmetric) two-segment-connected triangular optical waveguide networks with perfect and broken integer waveguide length ratios respectively. It is found that the number and the corresponding frequencies of the extremum spontaneous $\mathcal{PT}$-symmetric breaking points are dependent on the waveguide length ratio. Near the extremum breaking points, ultrastrong extraordinary transmissions are created and the maximal can arrive at, respectively, 2.4079×10^{14} and 4.3555×10^{13} in both kinds of networks. However, bidirectional invisibility can only be produced by the networks with broken integer waveguide length ratio, whose mechanism is explained in detail from the perspective of photonic band structure. The findings of this work can be useful optical characteristic control in the fabrication of $\mathcal{PT}$-symmetric optical waveguide networks, which possesses great potential in designing optical amplifiers, optical energy saver devices, and special optical filters.

Keywords: parity-time symmetry, optical waveguide network, integer broken ratios

PACS: 42.15.Eq, 42.25.Bs, 42.82.Et **DOI:** 10.1088/1674-1056/ab3f92

1. Introduction

In the recent two decades, a kind of absorbing artificial optical structures to control and confine the propagation of electromagnetic (EM) waves, the $\mathcal{PT}$-symmetric systems, have been widely investigated. In quantum mechanics, the eigenvalues of observable mechanical quantities must be real numbers, therefore their operator matrices should be Hermitian ones. Bender *et al.*[1–4] found in the year 1998 that for a $\mathcal{PT}$-symmetric system, even if its Hamiltonian is non-Hermitian, when the potential function is smaller than a certain threshold, all energy eigenvalues are still real numbers. When the potential function is larger than this threshold, its energy eigenvalues appear complex numbers. This threshold is called spontaneous $\mathcal{PT}$-symmetric breaking point. In 2007, El-Ganainy *et al.*[5–9] introduced the concept of $\mathcal{PT}$-symmetry into optical system through paraxial approximation. Similar to the $\mathcal{PT}$-symmetric mechanical system, $\mathcal{PT}$-symmetric optical systems can produce extraordinary optical features and phenomena near the spontaneous $\mathcal{PT}$-symmetric breaking point. Subsequently, $\mathcal{PT}$-symmetric optical systems, such as $\mathcal{PT}$-symmetric optical lattices,[6–10] optical waveguides,[11–29] inhomogeneous nonlinear optical media,[30] and graphene,[31,32] have been widely investigated and some extraordinary optical characteristics, for instance, birefringence,[6] unidirectional invisibility,[8,9] ultrastrong absorption,[31] and single-mode lasing,[33,34] have been found.

Optical waveguide networks (OWNs)[35–52] are another type of novel artificial optical structures to manipulate the propagation of EM waves. It is found that they can produce ultrastrong photonic localization,[31] extreme wide photonic bandgap (PBG),[38,41,44] interesting comb-like optical transmission spectrum,[45,46] rich photonic attenuation mode,[49] and so on. However, studies that combine the idea of optical $\mathcal{PT}$-symmetry and OWNs are quite rare.

Recently, our research group designed a $\mathcal{PT}$-symmetric aperiodic Thue–Morse optical waveguide network[53] and a $\mathcal{PT}$-symmetric periodic ring waveguide network,[54] whose waveguide length ratios are perfect integer ratios (i.e., 1 : 1, 1 : 2, 1 : 3, ...). Although seemingly similar, the difference between $\mathcal{PT}$-symmetric optical lattices[6–10] and $\mathcal{PT}$-symmetric optical waveguide networks are fundamental. The former possesses a pair of gain and loss waveguides which are coupled perpendicularly to the directional of light propagation; the latter arranges the gain and loss profiles alternately along the length, whose waveguide segments and unit cells are all physically linked and connected.

In the previous studies of $\mathcal{PT}$-symmetric optical waveguide networks, it is found that the maximal extraordinary

*Project supported by the National Natural Science Foundation of China (Grant Nos. 11674107, 61475049, 11775083, 61875057, 61774062, and 61771205) and Special Funds for the Cultivation of Guangdong College Students' Scientific and Techonlogical Innovation, China (Grant No. pdjhb0139).

†These authors contributed equally to this work.

‡Corresponding author. E-mail: xbyang@scnu.edu.cn

© 2019 Chinese Physical Society and IOP Publishing Ltd

transmission of the periodic one is several orders of magnitude larger than that of the aperiodic one, and the determination of the extremum spontaneous $\mathcal{PT}$-symmetric breaking point is much simpler for the periodic one than that for the aperiodic one. Therefore, in this work, we focus on the $\mathcal{PT}$-symmetric periodic waveguide network. Besides, through the study of dieletric OWNs,[39–46,49,52] it is found that the PBG, photonic localization, and transmission change dramatically with variation of waveguide length ratio from perfect to broken integer ratio. The perfect integer ratio represents the form of $1:z$ with z being a small integer, while the broken integer ratio denotes the form of $1:z-\delta$ with δ being a very small positive number like 0.1, 0.01, 0.001, ... With such waveguide length ratio, a very narrow passband can be created near the center of the wide stopband and a very narrow stopband can be created near the center of the wide passband. Hence, when the waveguide length ratios of the $\mathcal{PT}$-symmetric periodic waveguide networks change from perfect to broken integer ratios, do the optical $\mathcal{PT}$-symmetry related characteristics change as well? Investigations on this question may deepen the community's understandings on the $\mathcal{PT}$-symmetric optical waveguide networks, and may be helpful for controlling and confining the propagation of EM waves.

In this study, we investigate the propagation properties of EM waves in one-dimensional $\mathcal{PT}$-symmetric two-segment-connected triangular optical waveguide networks with perfect and broken integer waveguide length ratios. It is found that the number and the corresponding frequencies of the extremum spontaneous $\mathcal{PT}$-symmetric breaking points are dependent on the degree of brokenness δ. Near the extremum breaking points, ultrastrong extraordinary transmissions are created and the maxima can arrive at 2.4079×10^{14} and 4.3555×10^{13} in the two kinds of networks, respectively, which are several orders of magnitude larger than those in the $\mathcal{PT}$-symmetric Thue–Mose waveguide networks[53] and $\mathcal{PT}$-symmetric periodic waveguide-ring networks.[54] However, bidirectional invisibility can only be produced by the networks with broken integer waveguide length ratios, whose mechanism is explained in detail from the perspective of photonic band structure. The findings of this work can be useful optical characteristic control in the fabrication of $\mathcal{PT}$-symmetric optical waveguide networks, which possesses great potential in designing optical amplifiers, optical energy saver devices, and special optical filters.

This paper is organized as follows. In Section 2, our designed model, the main theory, and the methods for analytical deduction and numerical calculation are demonstrated and introduced. In Section 3, we show the distribution of photonic modes. The numerical and analytical discussions of the extremum breaking points, the transmission and reflection characteristics of the networks with perfect and broken integer waveguide length ratios are demonstrated. Section 4 gives the conclusion of this work.

2. Model and methods

2.1. The optical structure

In this article, the schematic diagram of our designed structure is plotted in Fig. 1. In this model, every two adjacent nodes of the same unit cell are connected by the two waveguide segments with the lengths of d_1 and d_2, respectively, with the shortest segment d_1 defined as a unit length "1", and the lengths of the other segments are expressed as a normalized value relative to d_1. Hence the waveguide length ratio is expressed as $d_1:d_2=1:t$, where it is called perfect integer ratio when $1:t=1:z$ and z itself is a small integer; broken integer ratio when a small positive number δ is subtracted and $1:t=1:z-\delta$. For example, the waveguide length ratios of $d_1:d_2=1:1,\ 1:2$ are perfect integer ratios and $d_1:d_2=1:0.999,\ 1:1.99$ are broken integer ratios with corresponding degrees of brokenness $\delta=10^{-3}$ and 10^{-2}, respectively. In this study, without loss of generality, the simplest form, the smallest odd and even numbers, $z=1,2$ are used to investigate the transmission and reflection behaviors in our designed model. In order to measure conveniently, d_1 is set to be related to the communication wavelength $\lambda_{\rm C}=1550$ nm. In Subsection 3.2, from Fig. 2 one can see that $\nu_{\rm GBP}\approx0.693=c/d_1$, where $\nu_{\rm GBP}$ is the frequency of the spontaneous $\mathcal{PT}$-symmetric generalized breaking point (GBP) of the networks with $d_1:d_2=1:1$, therefore we set $\nu_{\rm GBP}=c/\lambda_{\rm C}$, and consequently, $d_1=0.693\lambda_{\rm C}\approx1074$ nm. Each waveguide is composed of three subsegments whose lengths m are all the same for simplicity, as shown in Fig. 1(b), and the refractive index of each waveguide segment is defined as follows:

$$n(x)=\begin{cases} n_1=n_{\rm R}+n_{\rm I}{\rm i}, & (0\le x\le a_{ij}),\\ n_2=n_{\rm R}, & (a_{ij}<x\le b_{ij}),\\ n_3=n_{\rm R}-n_{\rm I}{\rm i}, & (b_{ij}<x\le l_{ij}),\end{cases}\tag{1}$$

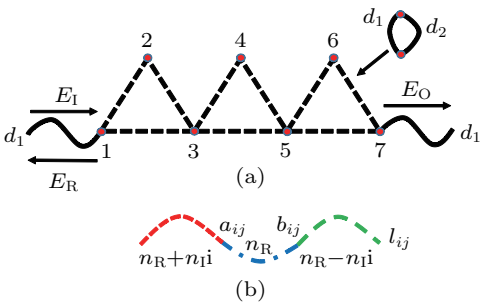


Fig. 1. Schematic diagram of the optical structure. (a) The optical waveguide network with three unit cells, one entrance, and one exit, where $E_{\rm I}$, $E_{\rm R}$, and $E_{\rm O}$ are, respectively, the input, reflected, and output EM waves. Each black thick dashed line represents two segments of $\mathcal{PT}$-symmetric waveguides with the lengths of d_1 and d_2, respectively, and the black thick solid curves at the entrance and exit represent $\mathcal{PT}$-symmetric waveguides with the length of d_1. (b) $\mathcal{PT}$-symmetric waveguide composed of three subsegments, where the lengths of the three subsegments are the same.

where $n_{\mathrm{R}} = n_{\mathrm{SiO_2}} = 1.4430$,[55,56] the optimal n_{I} value is determined by the extremum spontaneous $\mathcal{PT}$-symmetric breaking point in Subsection 3.2, and silicon dioxide (SiO_2) is chosen to be the material of the three subsegments. a_{ij}, $b_{ij}-a_{ij}$, and l_{ij} are, respectively, the lengths of the first sub-segment, the second sub-segment, and the whole waveguide segment between nodes i and j.

2.2. Network equation

In this research, each waveguide in the networks is composed of three materials, therefore, a three-material network equation is needed to study their photonic modes, transmissions, and reflections. As is known to all, the EM wave function in 1D waveguide segment between nodes i and j can be regarded as a linear combination of two opposite traveling plane waves

$$\psi_{ij} = \begin{cases} \alpha_1 \mathrm{e}^{\mathrm{i}k_1 x} + \beta_1 \mathrm{e}^{-\mathrm{i}k_1 x}, & (0 \le x \le a_{ij}), \\ \alpha_2 \mathrm{e}^{\mathrm{i}k_2 x} + \beta_2 \mathrm{e}^{-\mathrm{i}k_2 x}, & (a_{ij} < x \le b_{ij}), \\ \alpha_3 \mathrm{e}^{\mathrm{i}k_3 x} + \beta_3 \mathrm{e}^{-\mathrm{i}k_3 x}, & (b_{ij} < x \le l_{ij}), \end{cases} \tag{2}$$

with the wave vector $k_u = \omega n_u / c$ $(u = 1,2,3)$. By means of the continuities of the wave function, its differential quotient and energy flux conservation, one can deduce the following three-material network equation:[53]

$$\begin{aligned} &\psi_i \sum_j \frac{AB\cos E_{ij} + CD\cos F_{ij} + BC\cos G_{ij} + AD\cos H_{ij}}{BC\sin G_{ij} + AD\sin H_{ij} - AB\sin E_{ij} - CD\sin F_{ij}} \\ &- \sum_j \psi_j \frac{4k_2k_3}{BC\sin G_{ij} + AD\sin H_{ij} - AB\sin E_{ij} - CD\sin F_{ij}} \\ &= 0, \end{aligned} \tag{3}$$

where ψ_i and ψ_j are the wave functions at nodes i and j, respectively,

$$\begin{cases} A = k_1 + k_2, \\ B = k_3 + k_2, \\ C = k_2 - k_1, \\ D = k_3 - k_2, \\ E_{ij} = a_{ij}(k_1 - 2k_2 + k_3) + l_{ij}k_2, \\ F_{ij} = a_{ij}(k_1 + 2k_2 - k_3) - l_{ij}k_2, \\ G_{ij} = a_{ij}(-k_1 - 2k_2 + k_3) + l_{ij}k_2, \\ H_{ij} = a_{ij}(-k_1 + 2k_2 + k_3) - l_{ij}k_2. \end{cases} \tag{4}$$

In the next section, by use of three-material network equations (3) and (4), the distribution of photonic modes, transmissions, and reflections of the networks are calculated and plotted.

3. Results and discussion

3.1. Photonic mode distribution

The generalized Floquet–Bloch theorem,[39] $\psi_{\boldsymbol{K}}(\boldsymbol{N}+\boldsymbol{T}) = \psi_{\boldsymbol{K}}(\boldsymbol{N})\mathrm{e}^{\mathrm{i}\boldsymbol{K}\cdot\boldsymbol{T}}$ can be used to assess the photonic mode distribution. In a periodic optical waveguide network, the difference between the wave functions of the N-th and the $(N+T)$-th unit cell is a phase factor of $\mathrm{e}^{\mathrm{i}\boldsymbol{K}\cdot\boldsymbol{T}}$. When $\boldsymbol{K}$ is real, $\boldsymbol{K}\cdot\boldsymbol{T}$ is also real. Therefore, the amplitude of the wave function is kept constant, while the phase changes by a factor of $\mathrm{e}^{\mathrm{i}\boldsymbol{K}\cdot\boldsymbol{T}}$. This mode is called ordinary propagation mode (OPM).[49] When $\boldsymbol{K} = K_{\mathrm{R}} + \mathrm{i}K_{\mathrm{I}}$ is a complex number, $\boldsymbol{K}\cdot\boldsymbol{T}$ is also complex. Subsequently, not only the phase changes by a factor of $\mathrm{e}^{\mathrm{i}K_{\mathrm{R}}\cdot T}$, but also the amplitude changes by a factor of $\mathrm{e}^{-K_{\mathrm{I}}\cdot T}$. When $K_{\mathrm{I}} > 0$, the amplitude of the wave function attenuates; when $K_{\mathrm{I}} < 0$, the amplitude gains. These two photonic modes are called, respectively, attenuation propagation mode (APM) and gain propagation mode (GPM), which are the non-propagation modes.

For infinite-unit-cell networks, based on the three-material network equations (3) and (4), and the generalized Floquet–Bloch theorem, the following dispersion relation can be deduced:

$$\cos K = f(\nu) = \frac{4M - N}{N + 2MN}, \tag{5}$$

where

$$\begin{aligned} M &= \left[\sum_{q=1}^{2} \frac{AB\cos E_{ijq} + CD\cos F_{ijq} + BC\cos G_{ijq} + AD\cos H_{ijq}}{BC\sin G_{ijq} + AD\sin H_{ijq} - AB\sin E_{ijq} - CD\sin F_{ijq}}\right]^2, \\ N &= \left[\sum_{q=1}^{2} \frac{4k_2k_3}{BC\sin G_{ijq} + AD\sin H_{ijq} - AB\sin E_{ijq} - CD\sin F_{ijq}}\right]^2. \end{aligned} \tag{6}$$

From Eq. (5), it can be found that, for 1D vacuum or dielectric triangular optical waveguide networks,[47,48] where the refractive indices of the materials are all real, the dispersion function $f(\nu)$ must be real. Therefore, for $f(\nu)$ being real and $|f(\nu)| < 1$, from Eqs. (5) and (6) it can be deduced that the Bloch wavevector K of the structure possesses real solutions, EM waves with the corresponding frequencies propagate as OPM and form passbands. For $|f(\nu)| > 1$, it can be deduced that K possesses a pair of complex conjugate solutions. Mathematically, EM waves within this frequency range operate simultaneously as APM and GPM. However, in vacuum or dielectric optical waveguide networks, there exists only attenuation but no gain mechanism. Consequently, from a physical perspective, the corresponding EM waves will propagate only as APM and create stopbands. This shows that $|f(\nu)| = 1$ is a critical point for the transition of the photonic modes in vacuum or dielectric optical waveguide networks.

For $\mathcal{PT}$-symmetric waveguide networks in which the refractive indices are complex, it can be deduced from Eqs. (5) and (6) that $f(\nu)$ is complex in the total range of frequency. For complex $f(\nu)$, K possesses a pair of complex conjugate solutions. In $\mathcal{PT}$-symmetric optical waveguides, there exist both attenuation and gain mechanisms, and consequently, EM waves will propagate as APM and GPM simultaneously. It is reported that $\mathcal{PT}$-symmetric breaking points are located at the boundary between the OPM and non-propagation modes. However, in our designed model, EM waves only propagate

as two kinds of non-propagation modes, APM and GPM, simultaneously, and they can not be distinguished from each other at anytime and anywhere. Therefore, spontaneous $\mathcal{PT}$-symmetric breaking points of our designed model can not be simply determined by APM and GPM.

Recent research found that $|f(\nu)| = 1$ can be chosen to be the critical value for different photonic modes in $\mathcal{PT}$-symmetric networks. The reason is that from Eqs. (5) and (6), when $|f(\nu)|$ is small, $\mathrm{Im}(\boldsymbol{K})$ might also be small, and extraordinary transmission with $T > 1.0$ can not be created. Only when $f(\nu)$ is sufficiently large, can $\mathrm{Im}(\boldsymbol{K})$ be very large and the extraordinary transmission with $T > 1.0$ be produced. Moreover, we define both APM and GPM produced by the $\mathcal{PT}$-symmetric waveguide network corresponding to $|f(\nu)| \leq 1$ as weak propagation modes (WPMs), and those corresponding to $|f(\nu)| > 1$ as strong propagation modes (SPMs). By this condition, spontaneous $\mathcal{PT}$-symmetric breaking points of the networks are defined as the imaginary part of the refractive index, n_{I}, located between WPM and SPM.

3.2. Extremum spontaneous $\mathcal{PT}$-symmetric breaking point

Generally, extraordinary optical characteristics of the system can be found near the spontaneous breaking points, the boundary between WPM and SPM. We define the extremum spontaneous breaking points as follows: (i) when $|f(\nu)| = 1$; (ii) the dispersion function $f(\nu)$ is continuous and non-differentiable. From numerical results, the systems will produce increasing extraordinary transmissions and reflections at the extremum breaking points, so the optical propagation characteristics near the extremum breaking points are mainly studied here.

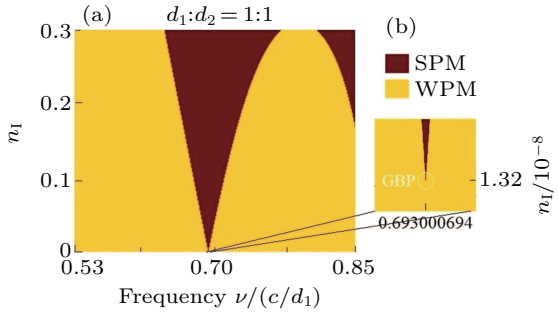


Fig. 2. Distribution of photonic modes in the network with $d_1 : d_2 = 1 : 1$, where SPM represents strong propagation mode, and WPM denotes weak propagation mode. (a) Overall figure; (b) enlarged figure of (a), where GBP indicates generalized breaking point.

By use of dispersion relation Eqs. (5) and (6), we can determine the photonic modes in the networks with perfect and broken integer waveguide length ratios. Since there are infinite configurations of networks with integer waveguide length ratios, for simplicity and without loss of generality, as a representative of the minimal odd number and the minimal even one, we study the networks with, respectively, $d_1 : d_2 = 1 : 1$ and $1 : 2$, whose photonic mode distributions are plotted in Figs. 2 and 3, where the yellow and red areas represent WPM and SPM, respectively. It can be seen from Fig. 2 that at the frequency of $\nu = 0.693000694c/d_1$, there exists one extremum spontaneous breaking point, where $n_{\mathrm{I}} = 1.32 \times 10^{-8}$. From Fig. 3, at the frequencies of $\nu = 0.57750053c/d_1$, $0.693000694c/d_1$, and $0.80850075c/d_1$, there exist three extremum spontaneous breaking points, where $n_{\mathrm{I}} = 1.02 \times 10^{-6}$, 1.25×10^{-8}, 1.34×10^{-6}, respectively.

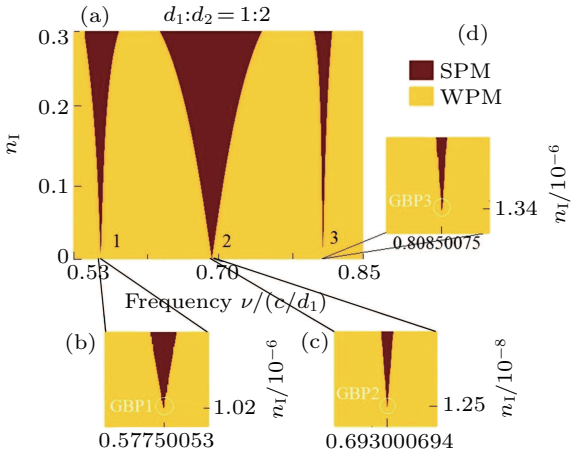


Fig. 3. Distribution of photonic modes in the network with $d_1 : d_2 = 1 : 2$: (a) overall figure; (b)–(d) enlarged figures of (a).

Through the previous study,[39] it is found that, for vacuum or dielectric OWNs, the width of the narrow band is proportional to the degree of brokenness δ in the broken integer waveguide length ratio. When δ decreases, the width of the narrow band will shrink and the characteristics of the networks will change dramatically. Therefore, in this work, we concentrate on the networks with $\delta < 10^{-2}$ as an example. However, there are infinite configurations of networks with broken integer waveguide length ratios. As an extension of the above two examples of perfect integer ratios, we study the networks with, respectively, $d_1 : d_2 = 1 : 0.99$ and $1 : 1.99$ (indicating $\delta = 10^{-2}$), whose photonic mode distributions are plotted in Fig. 4.

When $d_1 : d_2 = 1 : 1$ changes to $1 : 0.99$, the result is plotted in Fig. 4(a). From Fig. 4(a), one can see that the extremum breaking point near $\nu = 0.6930c/d_1$ disappears. When $d_1 : d_2 = 1 : 2$ changes to $1 : 1.99$, the result is plotted in Fig. 4(b). From Fig. 4(b), one can see that the extremum breaking point near $\nu = 0.6930c/d_1$ also disappears. The extremum breaking points originally located at $\nu = 0.57750053c/d_1$ and $0.80850075c/d_1$ are right-shifted, where ν becomes, respectively, $0.57942376c/d_1$ and $0.81120487c/d_1$. Besides, the values of n_{I} of the extremum breaking points also change from 1.02×10^{-6} and 1.34×10^{-6} to 7.20×10^{-7} and 1.82×10^{-6}, respectively.

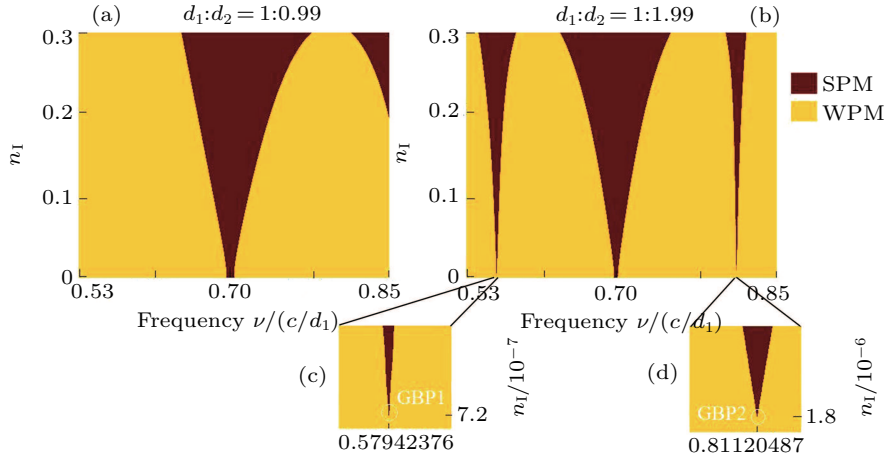


Fig. 4. Distribution of photonic modes in the networks with (a) $d_1 : d_2 = 1 : 0.99$, $\delta = 10^{-2}$; and (b) $d_1 : d_2 = 1 : 1.99$, $\delta = 10^{-2}$; (c) and (d) enlarged figures of (b).

Comparing Figs. 2–4, it is known that within the same frequency range, when the waveguide length ratios change from perfect to broken integer ratio, not only the number of the extremum breaking points reduces, but also the frequencies and the corresponding n_I of the extremum breaking points change. In Subsection 3.3, we will determine the optimal n_I according to the positions of the extremum breaking points, and then calculate the transmission and reflection near the corresponding frequency.

3.3. Extraordinary transmission and reflection in network with perfect integer waveguide length ratio

In previous studies of $\mathcal{PT}$-symmetric periodic waveguide ring networks, it is found that the ultrastrong extraordinary transmission and reflection are produced near the extremum breaking points, located between the red and yellow areas. We also find the same characteristics in our designed model in this study, and the transmission and reflection can reach maximum when the network possesses one unit cell. Therefore in Fig. 5, we plot the ultrastrong extraordinary transmission and reflection at the extremum breaking points in the networks with one unit cell, where the blue solid line, thin red dotted line, thick green dotted line, and brown dashed line denote the left-incident transmission, left-incident reflection, right-incident transmission, and right-incident reflection, respectively.

When $d_1 : d_2 = 1 : 1$, the results are shown in Fig. 5(a). From Fig. 5(a), one can see that (i) at the frequency of $\nu = 0.693000691c/d_1$, for the left-incident EM waves, the maximal transmission arrives at 2.4079×10^{14}; (ii) at the frequency of $\nu = 0.693000695c/d_1$, for the right-incident EM waves, the maximal transmission arrives at 1.2074×10^{13}; (iii) at the frequency of $\nu = 0.693000693c/d_1$, for both left- and right-incident EM waves, the minimal transmission arrives at 9.0025×10^{-10}.

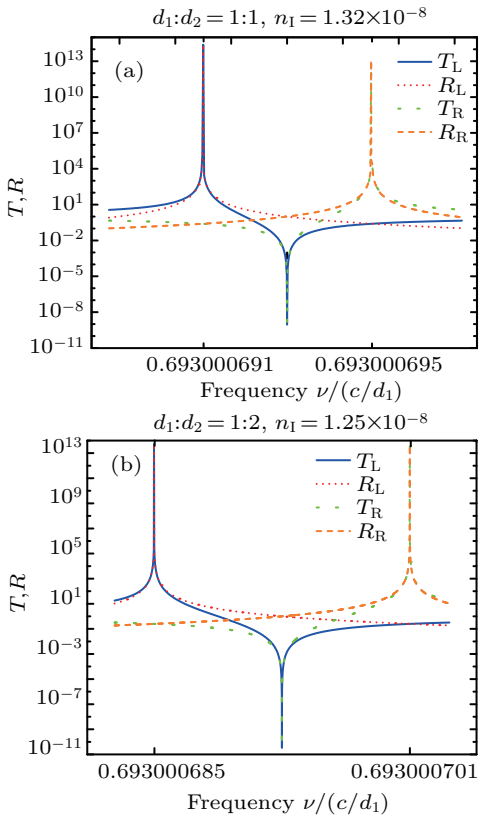


Fig. 5. Transmission and reflection spectra of the networks with perfect integer waveguide length ratios at extraordinary point, where the blue solid line, thin red dotted line, thick green dotted line, and brown dashed line represent the left-incident transmission and reflection and the right-incident transmission and reflection, respectively: (a) $d_1 : d_2 = 1 : 1$ and $n_I = 1.32 \times 10^{-8}$; (b) $d_1 : d_2 = 1 : 2$ and $n_I = 1.25 \times 10^{-8}$.

When $d_1 : d_2 = 1 : 2$, the results are shown in Fig. 5(b). From Fig. 5(b), one can see that (i) at the frequency of $\nu = 0.693000685c/d_1$, for the left-incident EM waves, the maximal transmission arrives at 5.2412×10^{13}; (ii) at the frequency of $\nu = 0.693000701c/d_1$, for the right-incident EM waves, the maximal transmission arrives at 4.2044×10^{13}; (iii) at the frequency of $\nu = 0.693000693c/d_1$, for both left- and right-incident EM waves, the minimal transmission arrives at 9.0036×10^{-10}. It means that the networks possess ultrastrong

extraordinary transmissions and ultrastrong PBG attenuation characteristics. Obviously, these networks may possess potential in designing optical filters, optical amplifiers, optical energy saver devices, and so on.

Similar to transmission, for both left- and right-incident EM waves, the transmission and reflection peaks totally overlap, no matter whether $d_1 : d_2 = 1 : 1$ or $1 : 2$. The difference between transmission and reflection is that the networks produce transmission valleys, but no reflection valley. These characteristics are completely different from those in the networks with broken integer waveguide length ratios shown in Subsection 3.4. Besides, for both transmission and reflection spectra, the left-incident curves do not coincide with the right-incident ones, these networks show typical nonreciprocity of EM wave propagation.

Regarding the reason why this structure can generate the extraordinary transmission and reflection, we believe it is a result of the extraordinary photonic modes mentioned in Section 3 and the gain-and-loss coupling resonant effect. (i) From the analysis on the photonic modes in Subsection 3.2, it is known that in our designed models, there exists no OPM, but two simultaneous non-propagation modes APM and GPM. These two modes are different from not only the OPM but also the non-propagation modes in normal dielectric waveguide networks. Therefore, in our models, neither passband nor stopband can be created, leading to completely different transmission and reflection spectra from those of dielectric ones. (ii) In $\mathcal{PT}$-symmetric networks, the pure gain and loss effects on photons of both gain and loss materials are all trivial and in subordinate roles, which means that they will neither cancel nor weaken one another, but strengthen and couple with each other. The gain and loss materials in such structure can be regarded as that they form a coupling resonant cavity and exhibit strong coupling resonant effect on APM and GPM photons, which, results in sharp transmission and reflection peak and valley, whose frequencies are determined inherently by the network structure as discussed in Section 3.

3.4. Extraordinary transmission and reflection in network with broken integer waveguide length ratio

In the above subsection, it is found that the networks with perfect integer waveguide length ratios can produce ultrastrong extraordinary transmission and reflection. Do the networks with broken integer waveguide length ratios possess the same characteristics? In this section, we discuss and analyze the propagation behavior of the networks with broken integer waveguide length ratios. In order to obtain increasing extraordinary transmission and reflection, we further reduce the degree of brokenness δ to produce an ultra-narrow photonic band. Without loss of generality, in this section we choose a very small $\delta = 10^{-8}$ to indicate a situation that the ratios are near-perfect, and design one-unit-cell networks with waveguide length ratios of $d_1 : d_2 = 1 : 1-\delta$ and $1 : 2-\delta$, ($\delta = 10^{-8}$), with $n_{\mathrm{I}} = 1.35 \times 10^{-8}$ and 1.26×10^{-8}, respectively.

When $d_1 : d_2 = 1 : 1-\delta$, $\delta = 10^{-8}$, the result is shown in Fig. 6. From Fig. 6, one can see that (i) at the frequencies of $\nu = 0.693000689c/d_1$ and $0.693000703c/d_1$, for the left-incident EM waves, the transmissions arrive at, respectively, 2.3127×10^{13} and 4.3555×10^{13}; (ii) for the right-incident EM waves, there is no transmission peak.

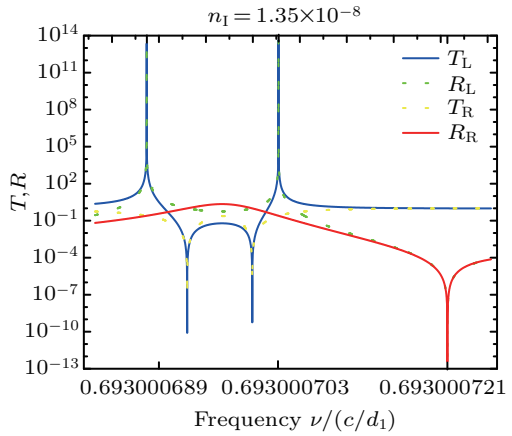


Fig. 6. Transmission and reflection spectra of the network with $d_1 : d_2 = 1 : 1-\delta$, $\delta = 10^{-8}$ at extraordinary point, with $n_{\mathrm{I}} = 1.35 \times 10^{-8}$, where the blue solid line, green dot line, yellow dot line, and red solid line indicate the left-incident transmission and reflection and the right-incident transmission and reflection, respectively.

When $d_1 : d_2 = 1 : 2-\delta$, $\delta = 10^{-8}$, the result is shown in Fig. 7. From Fig. 7, one can see that (i) at the frequencies of $\nu = 0.6930006892079c/d_1$ and $0.6930006935281c/d_1$, for the left-incident EM waves, the transmissions arrive at, respectively, 3.77056×10^{13} and 3.29120×10^{12}; (ii) at the frequencies of $\nu = 0.6930006935961c/d_1$ and $0.693000696363c/d_1$, for the right-incident EM waves, the transmissions arrive at, respectively, 3.88015×10^{12} and 6.86564×10^{13}. Obviously, the networks with broken integer waveguide length ratios also produce ultrastrong transmission and reflection, which also possess the potential in designing high efficiency optical filters, optical amplifiers, optical energy saver devices, and so on.

For both left- and right-incident EM waves, the transmission and reflection peaks totally overlap, no matter whether $d_1 : d_2 = 1 : 1-\delta$ or $1 : 2-\delta$. The networks with broken integer waveguide length ratios not only generate transmission and reflection peaks, but also produce reflection valleys which are absent in networks with perfect integer length ratios. From Fig. 6, one can see that there exists a reflection valley at the frequency of $\nu = 0.693000721c/d_1$, for left- and right-incident EM waves, where the reflections arrive at 3.5966×10^{-13} and 4.0859×10^{-13} and the transmissions arrive at 0.99995 and 1.00005, respectively. From Fig. 7, one

can see that there exists a reflection valley at the frequency of $\nu = 0.6930006935551c/d_1$, for left- and right-incident EM waves, where the reflections arrive at 3.31537×10^{-11} and 1.59481×10^{-13} and the transmissions arrive at 0.99995 and 1.00005, respectively. It means that this kind of networks have bidirectional invisibility characteristics, which may be useful in designing structures that are invisible to certain frequencies of EM waves.

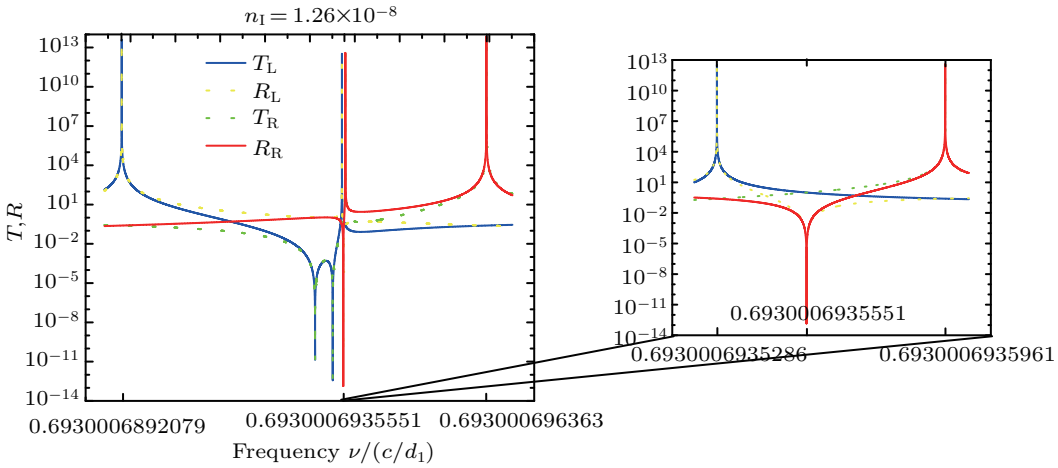


Fig. 7. Transmission and reflection spectra of the network with $d_1 : d_2 = 1 : 2-\delta$, $\delta = 10^{-8}$ at extraordinary point, with $n_I = 1.26 \times 10^{-8}$, where the blue solid line, green dot line, yellow dot line, and red solid line donate the left-incident transmission and reflection and the right-incident transmission and reflection, respectively.

Comparing Figs. 5–7, it is found that the networks with perfect integer length ratios can produce reflection valleys while those with perfect integer length ratios cannot. By use of dispersion relation Eqs. (5) and (6), we plot the band structure diagram of one dimensional two-segment connected triangular optical waveguide networks with uniform SiO_2 waveguide segments in Fig. 8, where $d_1 : d_2 = 1 : 1$, $1 : 0.99$ ($\delta = 10^{-2}$), $1 : 2$, and $1 : 1.99$ ($\delta = 10^{-2}$), respectively, to aid the explanation in the case of $\delta = 10^{-8}$. Based on the band structure diagram, the reflection valleys of the broken integer length ratio networks can be explained.

From Figs. 8(a) and 8(c), one can see that there exists a wide passband near the point of $\nu = 0.693c/d_1$ when $d_1 : d_2 = 1 : 1$ and $1 : 2$. When the networks are composed of uniform SiO_2, at the wide passbands, the transmission generally satisfies $0.01 \leq T \leq 1$ and changes slightly; the reflection commonly satisfies $0.01 \leq R + T \leq 1$ and also changes slightly. Consequently, the network can not produce a deep reflection valley. Therefore, when the uniform SiO_2 is replaced by the $\mathcal{PT}$-symmetric materials, the networks possess no enormously deep reflection valley as well. From Figs. 8(b) and 8(d), one can see that there exist a narrow stopband near the point of $\nu = 0.693c/d_1$ when $\delta = 10^{-2}$. The previous research[39,48] found that the width of the stopband is proportional to the degree of brokenness δ. Therefore, when $\delta = 10^{-8}$, we speculate that there exists an ultra-narrow stopband near the frequency of $\nu = 0.693c/d_1$. The boundary between ultra-narrow stopband and wide passband can be regarded as ultra-narrow passband for the reason that their transmission spectra are similar. When the networks are composed of uniform SiO_2, the propagation behaviors of extremely narrow passband and wide passband are different. Although the transmissions in wide and ultra-narrow passbands are both in the range of 0.01–1, with the variation from the ultra-narrow stopband to the ultra-narrow passband, the transmission changes enormously, therefore, the reflection

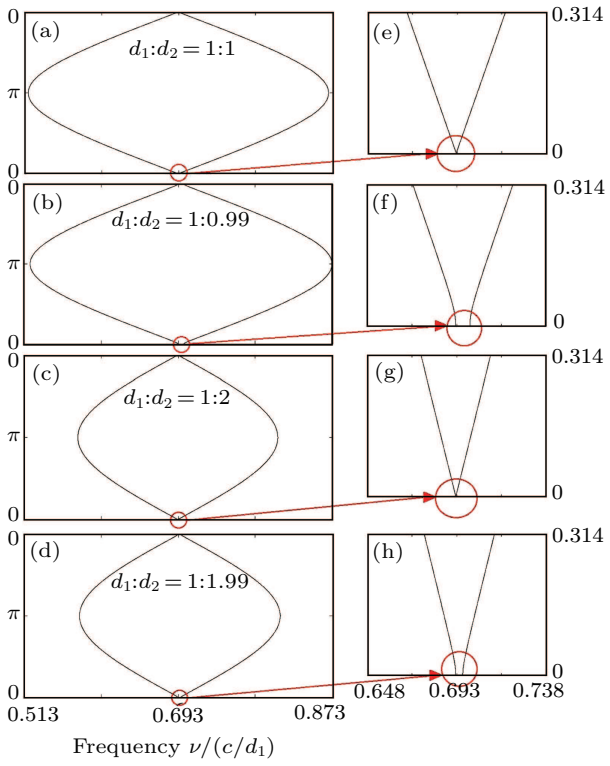


Fig. 8. The frequency band structure of one-dimensional two-segment connected triangular optical waveguide networks with perfect and broken integer waveguide length ratios: (a) $d_1 : d_2 = 1 : 1$; (b) $d_1 : d_2 = 1 : 0.99$ ($\delta = 10^{-2}$); (c) $d_1 : d_2 = 1 : 2$; (d) $d_1 : d_2 = 1 : 1.99$ ($\delta = 10^{-2}$); (e)–(h) enlarged figures of (a)–(d).

also changes greatly. When the networks are composed of $\mathcal{PT}$-symmetric materials, the resonance coupling effect of the gain and loss materials cause these changes in reflection to be magnified. This magnifying effect leads the reflection within the ultra-narrow passband to be exceedingly small, which results in an enormously deep reflection valley. It can be seen that the band structure is not only suitable for the optical waveguide network of vacuum/ordinary dielectric material, but also suitable for the $\mathcal{PT}$-symmetric optical waveguide network. Due to the same mechanism, similar transmission and reflection behaviors can be found in networks with a negative degree of brokenness δ, with the same number of transmission peaks and valleys and the same amount of spectral shift in opposite directions.

4. Conclusion

In this paper, we design the one-dimensional $\mathcal{PT}$-symmetric two-segment-connected triangular optical waveguide network and investigate its extraordinary optical characteristics. We obtain the network equation of the general three-material OWN and then thoroughly investigate the photonic modes in our designed networks with perfect and broken integer waveguide length ratios based on this network equation and the generalized Floquet–Bloch theorem. According to the photonic modes redivided as WPM and SPM, we find the extremum $\mathcal{PT}$-symmetric breaking points in periodic networks and study the transmissions and reflections near the extremum $\mathcal{PT}$-symmetric breaking points.

It is found that: (i) no matter whether the waveguide length ratios are perfect or broken integer ratios, the networks possess extremum $\mathcal{PT}$-symmetric breaking points. When the waveguide length ratios change from perfect or broken integer ratio, some $\mathcal{PT}$-symmetric extremum breaking points disappear, the frequencies and n_1 of the $\mathcal{PT}$-symmetric extremum breaking points change as well. (ii) The maximal transmission in the waveguide network with integer waveguide length ratio reaches 2.4079×10^{14} and the maximal reflection reaches 1.2074×10^{13}. These networks can produce extraordinary ultrastrong transmissions and reflections and they may possess potential application in the designing of all-optical devices, such as efficient photonic energy storages, optical amplifiers, optical filters, and so on. (iii) The networks with broken integer waveguide length ratios can not only produce extraordinary ultrastrong transmissions and reflections, but also generate reflection valleys, where the maximal transmission and reflection reach, respectively, 3.77056×10^{13} and 6.86564×10^{13}, and the minimal reflection reaches 4.0859×10^{-13}. It may be useful in designing structures that are invisible to certain frequencies of EM waves.

Finally, we explain the phenomena that reflection valleys appear in networks with broken integer waveguide length ratios based on the band structure diagram of one dimensional two-segment connected triangular optical waveguide networks with uniform SiO_2. It may deepen the community's understanding on $\mathcal{PT}$-symmetric optical waveguide networks.

References

[1] Bender C M and Boettcher S 1998 *Phys. Rev. Lett.* **80** 5243
[2] Bender C M, Brody D C and Jones H F 2002 *Phys. Rev. Lett.* **89** 270401
[3] Bender C M, Brody D C, Jones H F and Meister B K 2007 *Phys. Rev. Lett.* **98** 040403
[4] Bender C M 2007 *Reports on Progress in Physics* **70** 947
[5] El-Ganainy R, Makris K G, Christodoulides D N and Musslimani Z H 2007 *Optics Lett.* **32** 2632
[6] Makris K G, El-Ganainy R, Christodoulides D N and Musslimani Z H 2008 *Phys. Rev. Lett.* **100** 103904
[7] Rüter C E, Makris K G, El-Ganainy R, Christodoulides D N, Segev M and Kip D 2010 *Nat. Phys.* **6** 192
[8] Ramezani H, Kottos T, El-Ganainy R and Christodoulides D N 2010 *Phys. Rev. A* **82** 043803
[9] Lin Z, Ramezani H, Eichelkraut T, Kottos T, Cao H and Christodoulides D N 2011 *Phys. Rev. Lett.* **106** 213901
[10] Regensburger A, Bersch C, Miri M A, Onishchukov G, Christodoulides D N and Peschel U 2012 *Nature* **488** 167
[11] Ding S and Wang G P 2012 *Appl. Phys. Lett.* **100** 151913
[12] Konotop V V, Shchesnovich V S and Zezyulin D A 2012 *Phys. Lett. A* **376** 2750
[13] Bludov Y V, Konotop V V and Malomed B A 2013 *Phys. Rev. A* **87** 013816
[14] Chamorro-Posada P 2014 *J. Opt. Soc. Am. B* **31** 2728
[15] Dai C, Wang Y and Zhang X 2014 *Opt. Express* **22** 29862
[16] Gupta S K and Sarma A K 2014 *J. Mod. Opt.* **61** 227
[17] Hang C, Zezyulin D A, Huang G, Konotop V V and Malomed B A 2014 *Opt. Lett.* **39** 5387
[18] Huang C, Ye F and Chen X 2014 *Phys. Rev. A* **90** 043833
[19] Feijoo D, Zezyulin D A and Konotop V V 2015 *Phys. Rev. E* **92** 062909
[20] Ge L, Makris K G, Christodoulides D N and Feng L 2015 *Phys. Rev. A* **92** 062135
[21] Jia Y, Yan Y, Kesava S V, Gomez E D and Giebink N C 2015 *ACS Photon.* **2** 319
[22] Alaeian H, Baum B, Jankovic V, Lawrence M and Dionne J A 2016 *Phys. Rev. B* **93** 205439
[23] Hang C, Zezyulin D A, Huang G and Konotop V V 2016 *IEEE J. Select. Top. Quantum Electron.* **22** 5
[24] Nguyen N B, Maier S A, Hong M and Oulton R F 2016 *New J. Phys.* **18** 125012
[25] Walasik W and Litchinitser N M 2016 *Sci. Rep.* **6** 19826
[26] Fu Y, Xu Y and Chen H 2016 *Opt. Express* **24** 1648
[27] Wu B, Wu B, Xu J, Xiao J and Chen Y 2016 *Opt. Express* **24** 16566
[28] Li H, Zhu X, Shi Z and Lai T 2017 *J. Opt. Soc. Am. B* **34** 709
[29] Wang J, Dong H Y, Wu R P H, Mok T C and Fung K H 2017 *Opt. Lett.* **42** 535
[30] Raju T S, Hegde T A and Kumar C N 2016 *J. Opt. Soc. Am. B* **33** 35
[31] Cao P, Yang X, Wang S, Huang Y, Wang N, Deng D and Liu C T 2017 *IEEE Photon. J.* **9** 1
[32] Sarısaman M and Tas M 2018 *J. Opt. Soc. Am. B* **35** 2423
[33] Hodaei H, Miri M A, Heinrich M, Christodoulides D N and Khajavikhan M 2014 *Science* **346** 975
[34] Feng L, Wong Z J, Ma R M, Wang Y and Zhang X 2014 *Science* **346** 972
[35] Zhang Z Q, Wong C C, Fung K K, Ho Y L, Chan W L, Kan S C, Chan T L and Cheung N 1998 *Phys. Rev. Lett.* **81** 5540
[36] Dobrzynski L, Akjouj A, Djafari-Rouhani B, Vasseur J O and Zemmouri J 1998 *Phys. Rev. B* **57** R9388
[37] Mir A, Akjouj A, Vasseur J O, Djafari-Rouhani B, Fettouhi N, Boudouti E H E, Dobrzynski L and Zemmouri J 2003 *J. Phys.: Conden. Matter* **15** 1593

[38] Cheung S K, Chan T L, Zhang Z Q and Chan C T 2004 *Phys. Rev. B* **70** 125104
[39] Wang Z Y and Yang X 2007 *Phys. Rev. B* **76** 235104
[40] Song H H and Yang X B 2010 *Chin. Phys. B* **19** 74213
[41] Lu J, Yang X, Zhang G and Cai L 2011 *Phys. Lett. A* **375** 3904
[42] Cai L, Yang X and Lu J 2011 *Journal of Electromagnetic Waves and Applications* **25** 147
[43] Lu J, Yang X and Cai L 2012 *Opt. Commun.* **285** 459
[44] Xiao Q, Yang X, Lu J and Liu C 2012 *Opt. Commun.* **285** 3775
[45] Yang X, Song H and Liu T C 2013 *Phys. Lett. A* **377** 3048
[46] Wang Y, Yang X, Lu J, Zhang G and Liu C T 2014 *Phys. Lett. A* **378** 1200
[47] Tang Z, Yang X, Lu J and Liu C T 2014 *Opt. Commun.* **331** 53
[48] Tang Z X, Yang X B, Lu J and Liu T C Y 2014 *Chin. Phys. B* **23** 044207
[49] Xu X, Yang X, Wang S, Liu T C and Deng D 2015 *Opt. Express* **23** 27576
[50] Hu X, Yang X and Deng D 2017 *IEEE Photon. J.* **9** 4700414
[51] Hu X, Yang X and Deng D 2017 *Phys. Lett. A* **381** 1241
[52] Wu J and Yang X 2019 *Annalen der Physik* **531** 1800258
[53] Wu J and Yang X 2017 *Opt. Express* **25** 27724
[54] Zhi Y, Yang X, Wu J, Du S, Cao P, Deng D and Liu C T 2018 *Photon. Res.* **6** 579
[55] Palik E D 1998 *Handbook of Optical Constants of Solids* (1st Edn.) (San Diego: Academic Press)
[56] Aleksandrova A, Monastyrskyi G, Flores Y and Ted Masselink W 2012 *Appl. Opt.* **51** 6789